

# Oxygen diffusion in nanostructured perovskites

P.V. Glyanenko <sup>a</sup>, Yu.M. Kamenetsky <sup>a</sup>, A.P. Nemudry <sup>a,1</sup>,  
I.L. Zhogin <sup>a,1</sup>, H.J.M. Bouwmeester <sup>b,1</sup>, Z.R. Ismagilov <sup>c</sup>

<sup>a</sup>*Institute of Solid State Chemistry and Mechanochemistry,  
630128 Novosibirsk, Russia*

<sup>b</sup>*Institute for Nanotechnology, University of Twente, The Netherlands*

<sup>c</sup>*Institute of Catalysis, 630090 Novosibirsk, Russia*

---

## Abstract

Nonstoichiometric perovskite-related oxides (such as ferrites and cobaltites, etc.) are characterized by fast oxygen transport at ambient temperatures, which relates to the microstructural texturing of these materials, consisting wholly of nanoscale microdomains.

We have developed an inhomogeneous diffusion model to describe the kinetics of oxygen incorporation into nanostructured oxides. Nanodomain boundaries are assumed to be the high diffusivity paths for oxygen transport whereas diffusion into the domains proceeds much slower. Using Laplace transform methods, an exact solution is found for a ramped stepwise potential, allowing fitting of the experimental data to theoretical curves (in Laplace transforms). A further model generalization is considered by introducing additional parameters for the size distribution of domains and particles.

The model has been applied for qualitative evaluation of oxygen diffusion parameters from the data on wet electrochemical oxidation of nano-structured perovskite  $\text{SrCo}_{0.5}\text{Fe}_{0.2}\text{Ta}_{0.3}\text{O}_{3-y}$  samples.

*Key words:* inhomogeneous oxygen diffusion; nanostructured perovskites  
*PACS:*

---

<sup>1</sup> zhogin@inp.nsk.su; nemudry@solid.nsk.su; h.j.m.bouwmeester@tnw.utwente.nl

## 1 Introduction

At high temperature grossly nonstoichiometric perovskite related oxides are solid state solutions with a high concentration of structural defects (oxygen vacancies, dopant ions, etc.). As temperature decreases, structural ordering occurs, producing either superstructures, in which defects are assimilated as structural elements, or complex microstructures with a high density of extended defects [1]. The formation of the latter microstructures may be described using the concept of oversaturated solid solutions having a miscibility gap: oversaturation due to cooling causes unmixing of the initially homogeneous solid solution. The unmixing can proceed either by spinodal decomposition or homogeneous/heterogeneous nucleation [2]. Stabilization of nano-sized domains occurs due to a decrease in mobility of the domain boundaries at  $T \leq 0.3 T_m$ . The mechanisms that are responsible for the enhanced thermal stability against microdomain growth are: (a) solute drag, (b) grain boundary segregation, (c) pinning by secondary phases and (d) chemical ordering [3]. Another approach to the explanation of intrinsic inhomogeneity of nonstoichiometric and doped oxides related to a strong tendency toward phase separation in systems with strongly correlated electrons. Electron conducting oxides with transition metals having different charges (for example,  $Mn^{3/4+}$ ,  $Co^{3/4+}$ ,  $Cu^{2/3+}$ , etc) and magnetic states can break into a stable state made out of nanoscale coexisting clusters because of complicated electron-phonon and magnetic interactions [4]. The Gibbs energy of such a submicro-heterogeneous (nanostructured) system is essentially influenced by the nature of the interface between matrix and nucleus. This interface may be coherent, semi coherent and incoherent. If the interface is coherent or semicoherent the system behaves as a homogeneous single phase in terms of diffraction. Microdomain-textured oxides exemplify such systems rather well [1]. As shown in [5], unmixing of nonstoichiometric and doped oxides with perovskite-related structures produces microdomains of 5–50 nm in size.

Nanostructured materials may show enhanced ionic conductivity owing to the high density of interfaces which are enriched by defects due to the formation of space charge layers [6] or reduction of coordination number of cations in the vicinity of interface [7].

Therefore, nonstoichiometric doped oxides with microdomain texture may provide conductive channels for enhanced oxygen diffusion along the microdomain boundaries [8,9]. Materials with high oxygen mobility are of interest for applications such as oxygen electrolytes, electrodes, sensors and membranes for oxygen separation [8].

Numerous experimental proofs of enhanced diffusion along grain boundaries (including radiography, [10,11,12]) have initiated theoretical investigations

of inhomogeneous diffusion in polycrystalline materials [13,14,15]. The first mathematical description of fast diffusion along grain boundaries accompanied by penetration into the grains by means of bulk diffusion (without phase transition though) is shown in [13,16]. In [17,18], a mathematical model of the two-phase oxidation of MDT nonstoichiometric perovskite has been considered. The crystal is conceived as an assembly of parallel domain boundaries, which are considered to be high diffusivity paths. Oxidation proceeds as a result of rapid oxygen transport along the domain boundaries and two-phase oxidation of the microdomains.

Unlike the previous papers, here we assume that oxidation of microdomains occurs as a result of one phase reaction. We employ a model for oxygen transport in the MDT perovskites in the course of single phase oxidation, assuming that diffusion along the nanodomain boundaries is much faster than diffusion into the domains. Since nanostructured perovskites exhibit fast oxygen transport even at room temperature, the model was applied for the evaluation of oxygen diffusion parameters from data of wet electrochemical oxidation of nano-structured perovskite  $\text{SrCo}_{0.5}\text{Fe}_{0.2}\text{Ta}_{0.3}\text{O}_{3-y}$  samples in 1M KOH at ambient temperatures.

Potentiostatic method [19,20] is considered to be a convenient tool for studying oxygen transport in perovskites (where electron conductivity far exceeds the ion one). In the present study we have used a version of this method.

## 2 Experimental

Kinetic studies were carried out for  $\text{SrCo}_{0.5}\text{Fe}_{0.2}\text{Ta}_{0.3}\text{O}_{3-y}$  nonstoichiometric perovskite. The samples were synthesized by solid state reaction from the corresponding metal oxides and carbonates with preliminary homogenization of the starting materials in a planetary ball mill. A stoichiometric mixture of the powders was calcined at 900 °C, pressed in pellets, annealed in air at 1400 °C for 6 hours and cooled in the furnace.

For kinetic studies, the sintered sample was annealed at 950 °C in a quartz ampoule in dynamic vacuum ( $P \sim 10^3$  Pa). After that, the quartz ampoule was closed and placed in water for rapid quenching of the sample to room temperature.

Experiments were performed at room temperature (25 °C) in potentiostatic mode (three electrode cell, 1M KOH electrolyte, Hg/HgO reference electrode) with working electrodes of polycrystalline material (17–18 mg) pressed into Pt grids along with 1 wt.% of Teflon and 15–20 wt.% of acetylene black. The working electrode was placed in a cell at the set temperature and was main-

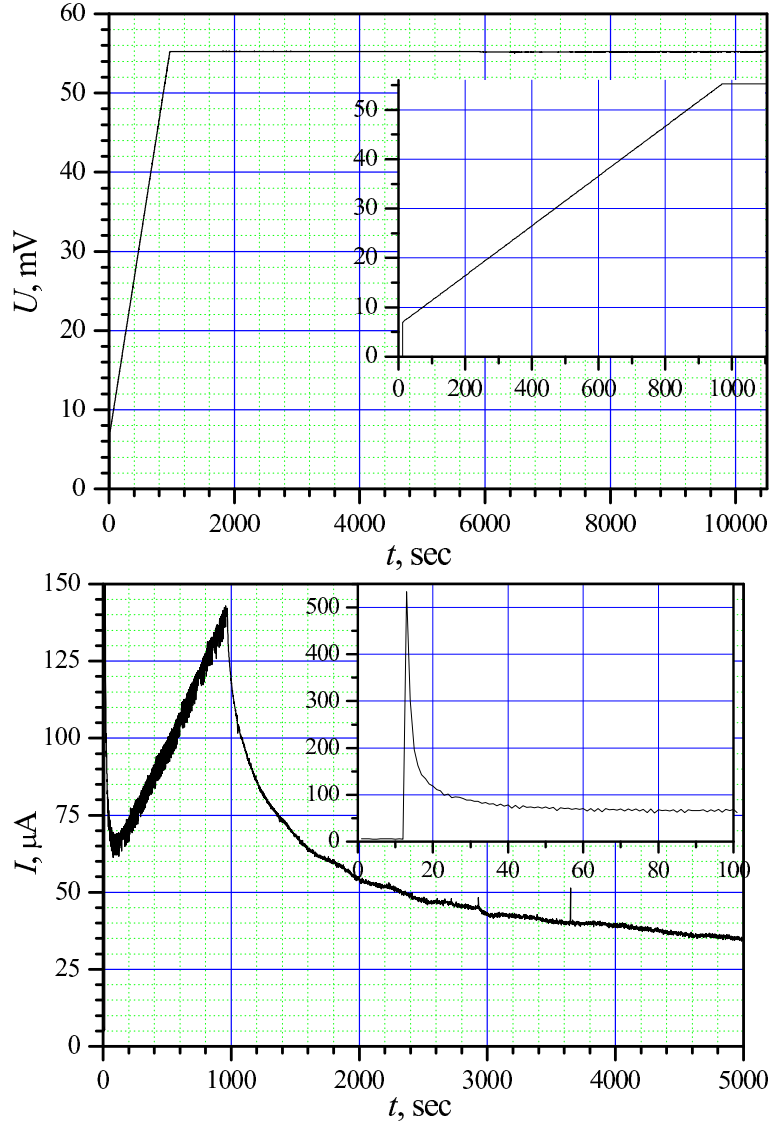


Fig. 1. Applied potential (a) and current (b) versus time.

tained up to an equilibrium potential  $U_0$ . At  $t = 0$  a voltage pulse between the working electrode and reference electrode has been applied. Re-equilibration through diffusion of oxygen into the working electrode material takes place. The rate of re-equilibration can be measured easily by monitoring the electric current passing through the cell, see Fig. 1.

### 3 Theoretical model

Similar to the model of spheres filling a half-space (grains in a thick metal plate, see [14]), we consider a model, where small spheres are inside large ones (nano-domains inside the perovskite powder particles). The simple geometry

of our model allows us to derive an exact solution for the current passing through the cell using the Laplace transform method.

Inverse Laplace transformation to determine the original function is not possible in analytical form (in analytical functions; this is the reason why one usually analyzes only the asymptotic current behavior at short and long times). Though there exist computational methods to do reverse Laplace transformations [21], they require intensive calculations (double Fourier transforms). Therefore, we have chosen another way of model comparison with experiment. After we perform numerical Laplace transformation of measured current function,  $J_{\text{exp}}(t)$ , (as well as potential function, if it is measured and is not given “analytically” with potentiostat) we adjust transform,  $\hat{J}_{\text{exp}}(p)$ , with model curves  $\hat{J}_{\text{th}}(p)$  (which depend on the applied potential profile).

However, computer inversion of Laplace transform may be useful for verifying the best approximation, or for the better choosing among several minima, if they occur.

A two-level model of spheres is used to describe the current passing through an electrochemical cell under potential of a chosen profile.

### 3.1 Diffusion in a spherical particle

The diffusion equation for a spherical particle, when the space derivatives (Laplacian) are reduced to differentiation over the radius, is written as follows:

$$\frac{\partial(xc)}{\partial t} = D \frac{\partial^2(xc)}{\partial x^2}. \quad (1)$$

Here  $c(t, x)$  is the concentration of the diffusing species,  $R$  the particle radius, and  $x$  the radial coordinate,  $0 \leq x \leq R$ . For initial and boundary conditions we have

$$c(t < 0, x) = 0, \quad c(t, x = R) = c_R(t).$$

Using the Laplace transform of  $c(t)$

$$\hat{c}(p, x) \equiv \int_0^{\infty} c(t, x) e^{-pt} dt$$

turns partial derivatives (1) into an ordinary differential equation

$$\frac{\partial^2(x\hat{c})}{\partial x^2} = \frac{p}{D}x\hat{c}. \quad (2)$$

Applying boundary condition,  $\hat{c}(p, R) = \hat{c}_R(p)$ , one can easily find the exact solution of equation (2),

$$\hat{c}(p, x) = \hat{c}_R(p) \frac{\kappa R}{\sinh(\kappa R)} \frac{\sinh(\kappa x)}{\kappa x}, \quad \kappa = \sqrt{p/D}. \quad (3)$$

Diffusion current (and electric one, if diffusing component carriers charge  $q$ ), passing through the whole particle boundary, may be expressed as follows:

$$J(t) = 4\pi q \int_0^R \frac{\partial c(t, x)}{\partial t} x^2 dx,$$

$$\hat{J}(p) = 4\pi q \frac{p\hat{c}_R(p) R}{\sinh(\kappa R)} \int_0^R \sinh(\kappa x) x dx. \quad (4)$$

One may expect that the diffusion coefficient is independent of concentration, provided that the oxygen content in the perovskite lattice changes only slightly, e.g.,  $\Delta y < 0.1$ . For this purpose the amplitude of potential pulse,  $U_A$ , applied to the cell, should be small enough (this is determined by the ratio of sample mass and charge). We assume that the access of oxygen ions to the particles is not limited and, hence, there is a linear dependence between concentration and the potential

$$c_R(t) \propto U(t) \text{ or } c_R(t)/c_A = U(t)/U_A.$$

In experiments we used potential steps of the following form (see Fig. 1a):

$$U(t)/U_A = H(t; h, t_0) \equiv \begin{cases} 0, & t < 0 \\ h + (1-h)t/t_0, & 0 \leq t \leq t_0 ; \\ 1, & t > t_0 \end{cases}$$

this gives the Laplace transform ( $0 \leq h \leq 1$ ):

$$p c_R(p)/c_A = h + (1-h)(1 - e^{-pt_0})/(pt_0) \quad (\xrightarrow{p \rightarrow 0} 1). \quad (5)$$

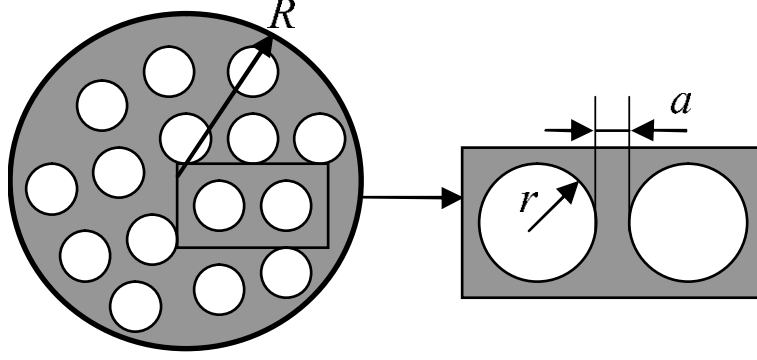


Fig. 2. Regions of slow (white) and fast (grey) diffusion

Introducing value  $Q \equiv \hat{J}(0) = 4\pi R^3 q c_A / 3$  for a total charge passed through the cell, and using equations (3), (4) and (5) we obtain ( $\tau \equiv R^2/D$  is a characteristic diffusion time for a sphere of radius  $R$ ;  $\sqrt{p\tau} = \kappa R$ )

$$\hat{J}(p)/Q = p c_R(p)/c_A F(\sqrt{p\tau}), \quad (6)$$

$$\text{where } F(y) \equiv \frac{3 \coth(y)}{y} - \frac{3}{y^2} \quad (y \rightarrow 0 \rightarrow 1 - y^2/15 + \dots). \quad (7)$$

### 3.2 Inhomogeneous diffusion model: spheres of two types

Let us imagine that particles in the sample are non-uniform (see Fig. 2) and contain domains of a typical size  $r$ , where diffusion rate is small,  $D_1$ , and well as regions neighboring with domains boundaries, where diffusion rate is high,  $D_2$ . More exactly, let us consider  $D_2$  as an effective diffusion coefficient for a porous particle, obtained, when all domains are removed, as if they are non-permeable for diffusion, i.e.  $D_1 = 0$ . This effective coefficient may change not only with temperature, but also with parameters related to the nano-domain structure, such as oxygen content, quenching rate, etc.

If diffusion coefficient  $D_1$  is small but not equal to zero, then diffusion equation should reflect oxygen incorporation inside the domains. One may assume that the concentration along the boundary of each domain is approximately the same (since transport to the boundary is fast) and is equal (or at least proportional) to the current local concentration:

$$c_{1r}(t) = c_2(x, t).$$

Therefore, we may write effective diffusion equation in a heterogeneous particle

instead of equation (1):

$$v_2 \left( \frac{\partial c_2}{\partial t} - D_2 \frac{\partial^2 (x c_2)}{x \partial x^2} \right) = -n_d J_1(t, x)/q.$$

Here  $n_d$  is the concentration of domains,  $J_1/q$  the diffusion current into a domain,  $v_1 = n_d 4\pi r^3/3$ ,  $v_2 = 1 - v_1$  are volume fractions for regions of slow and fast diffusion, respectively. After Laplace transformation we obtain (taking into account equations (5), (6)):

$$\frac{\partial^2 (x \hat{c}_2)}{\partial x^2} = \frac{p}{D_2} x \hat{c}_2 (1 + \alpha F(\sqrt{p\tau_1})), \quad (8)$$

where  $\alpha = v_1/v_2$  is the ratio of above mentioned volume fractions (see Fig. 2).

As it is mentioned in [14], equilibrium concentrations (of diffusant) along the boundaries and inside the domains (i.e. grains) may not coincide. Therefore, dimensionless parameter  $\alpha$  may include not only geometry but also the concentration factor.

One may derive the final expression for the current using equation (8) (it is necessary to remember that the particle is inhomogeneous):

$$\begin{aligned} \hat{J}(p) &= 4\pi R^2 D_2 \left. \frac{\partial \hat{c}_2}{\partial x} \right|_{x=R} \\ &= Q \frac{p \hat{c}_{2R}(p)}{c_A} \frac{1 + \alpha f(p\tau_1)}{1 + \alpha} f(p\tau_2 [1 + \alpha f(p\tau_1)]). \end{aligned} \quad (9)$$

Here notations  $f(y) \equiv F(\sqrt{y})$ ,  $\tau_1 \equiv r^2/D_1$ ,  $\tau_2 \equiv R^2/D_2$  (see equations (5)–(7)) are introduced.

### 3.3 Assembly of particles, particle size distribution

If powder particles are of different sizes, then the current expression (6) and expression (9) should be integrated with the function of volume (mass) distribution of particles,  $M(R)$  (norm per unit):

$$\hat{J}(p)/Q = \frac{p \hat{c}_R(p)}{c_A} \int_0^\infty F(\kappa R) M(R) dR.$$



If the ‘relative’ dispersion of the distribution,

$$\Delta_R = \langle (R - R_0)^2 \rangle / R_0^2 \quad (R_0 = \langle R \rangle),$$

is small, we leave the first correction term, changing functions in (9) or (6) as follows (prime means differentiation by argument):

$$F(\kappa R) \rightarrow F^*(\kappa R_0) = F(\kappa R_0) + (\kappa R_0)^2 F''(\kappa R_0) \Delta_R / 2, \quad (10)$$

where  $y^2 F''(y) = 6(1 + y^2 / \sinh^2 y)(1 + y / \tanh y) - 24/y^2$ .

One may obtain this correction by e.g. integration with formal distribution (delta functions):

$$M(R) = \delta(R - R_0) + \delta''(R - R_0) \Delta_R R_0^2 / 2,$$

which has proper first two moments. Saddle-point integration with the Gaussian distribution  $M(R) \propto \exp(-(R/R_0 - 1)^2 / 2\Delta_R)$  gives the same result.

In the similar manner one may correct for the size dispersion of nano-domains,  $\Delta_r$ .

## 4 Experimental results and computation

According to the X-ray diffraction (Fig. 3) and iodometric titration data, quenched samples of  $\text{SrCo}_{0.5}\text{Fe}_{0.2}\text{Ta}_{0.3}\text{O}_{3-y}$  had the expanded cubic unit cell parameters (from 3.934 Å to 3.952 Å) and reduced oxygen content (from 2.92 to 2.70) with respect to slowly cooled ones.

XRD suggests single phase behaviour, while the HREM data shows that the samples possess a micro-domain texture (Fig. 4) with a typical domain size of about 10 nm.

The mechanism of electrochemical oxidation of  $\text{SrCo}_{0.5}\text{Fe}_{0.2}\text{Ta}_{0.3}\text{O}_{3-y}$  has been studied with chronopotentiometry combined with *in situ* X-ray diffraction. The results of evaluation of the *in situ* data are shown in Fig. 5. Monotonous changes in the unit cell parameters and potential vs. inserted oxygen (x) ( $x = n/2$ , where  $n$  is a charge transfer) provide evidence of one phase mechanism of oxidation [22].

For kinetic studies, the samples were powdered, and particle size distribution was measured (see Fig. 6).

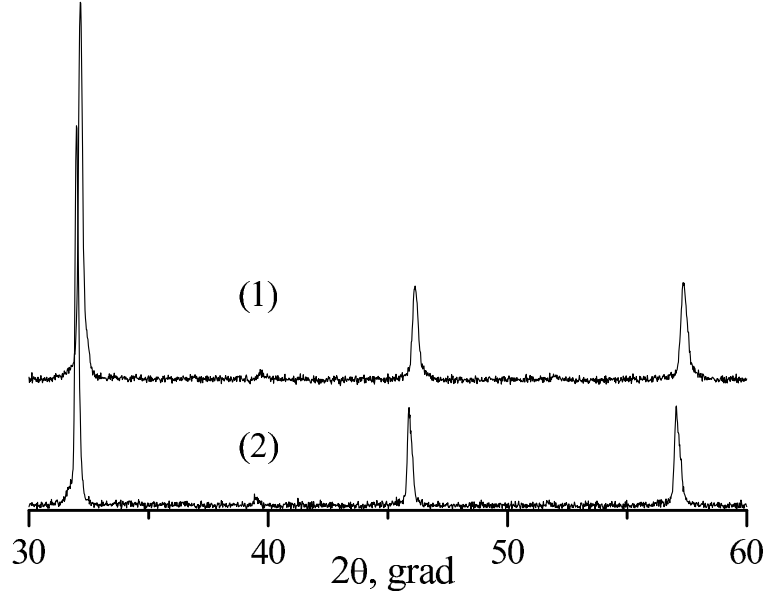


Fig. 3. Diffraction patterns of samples  $\text{SrCo}_{0.5}\text{Fe}_{0.2}\text{Ta}_{0.3}\text{O}_{3-y}$ : (1) as sintered, (2) after annealing at 950 °C and quenching in vacuum ( $P \sim 10^3$  Pa).

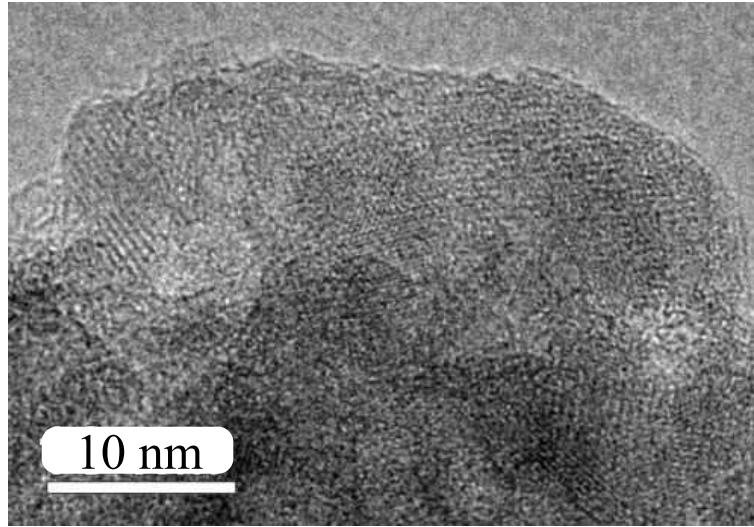


Fig. 4. High resolution image of  $\text{SrCo}_{0.5}\text{Fe}_{0.2}\text{Ta}_{0.3}\text{O}_{2.7}$  sample possessing microdomain texture.

Fig. 1 shows  $U(t)$  and  $J_{\text{exp}}(t)$  functions *versus* time, obtained in one of experiments. The time of current measurement averaging was 1 second. This obstacle somewhat distorted the current plot at short times.

Computations were performed in MatLab. For the data, presented in Fig. 1, potential step parameters are the following (see equations (5) and (9)):

$$h = 7/55.25; t_0 = 958; \% \text{ sec}$$

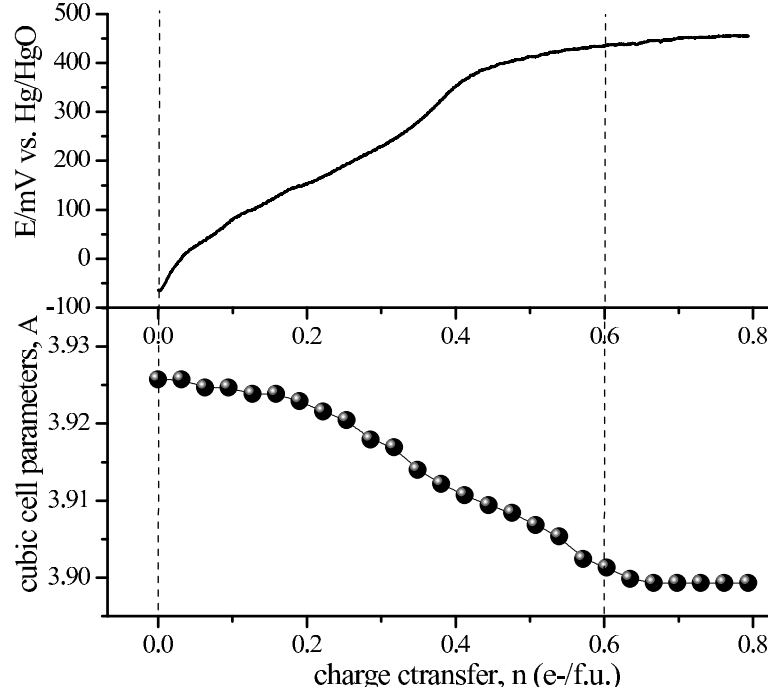


Fig. 5. In situ anodic oxidation of  $\text{SrCo}_{0.5}\text{Fe}_{0.2}\text{Ta}_{0.3}\text{O}_{2.7+x}$ : (a) potential  $E$  vs. charge transfer  $n$ , (b) change of unit-cell parameters with  $n$ ,  $n/2 = x$ .

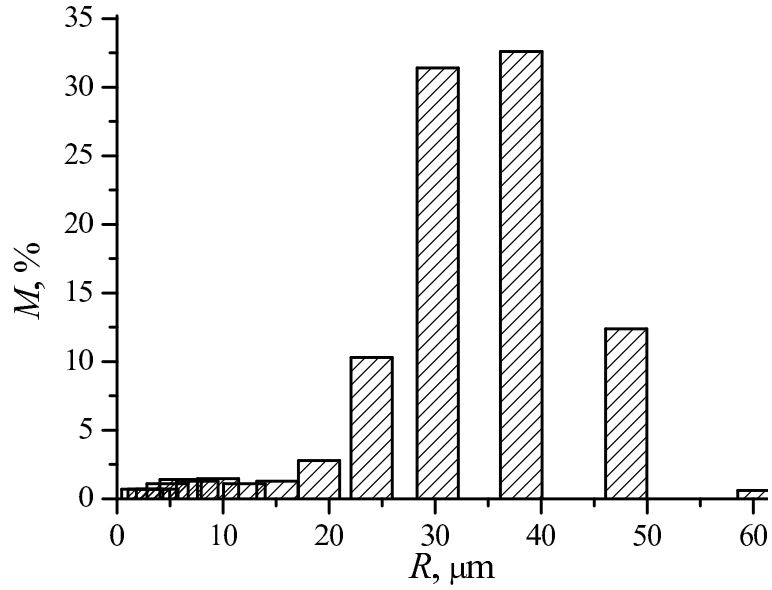


Fig. 6. Mass distribution of particles over size.

After  $\hat{J}_{\text{exp}}(p)/Q$  was calculated (exponential slope at long times ( $t > 3000$  s) was considered analytically), correction for the time of micro ammeter integration (1 s) was introduced:

$$J_{\text{ep}} = J_{\text{ep}} \cdot p / (1 - \exp(-p));$$

Then optimization over three parameters entering the model function of cur-

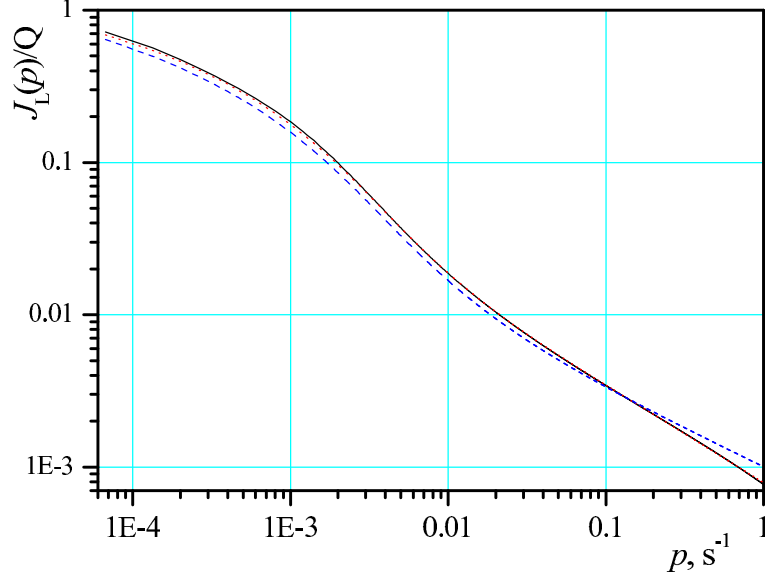


Fig. 7. Normalized Laplace transform of experimental data (solid;  $Q = 0.44$  C) and fitting model curves for inhomogeneous (dot) and homogeneous (dash;  $\alpha = 0$ ) model.

rent (equation (9)) was done:

```

par0 = [tau1,tau2,alpha];
options = optimset('TolFun',1e-10,'TolX',1e-6, ...
    'MaxFunEvals',1e3,'MaxIter',1e3);
[par1,fval,exitflag,output] = ...
    fminsearch('diff_fun',par0,options,p,Jep,handle);
...
function ff = diff_fun(param,p,Jep,handle)
...
ff = sum(abs(Jtp - Jep));

```

Computing results are shown in Fig. 7, model parameters for theoretical curve (dotted line) being as follows:

$$\tau_1 = 49 \text{ s}, \quad \tau_2 = 19 \cdot 10^3 \text{ s}, \quad \alpha = 4.8.$$

Using values  $R = 32 \mu\text{m}$ ,  $r \sim 10 \text{ nm}$ , one may estimate diffusion coefficients

$$D_2 = 5 \cdot 10^{-10} \text{ cm}^2/\text{s}, \quad D_1 = 2 \cdot 10^{-13} \text{ cm}^2/\text{s}.$$

Let us note that fitting by the homogeneous model gives essentially larger errors (see dashed curve in Fig. 7), and yields another value:  $\tau_2 = 15 \cdot 10^4 \text{ s}$ .

## 5 Discussion and conclusions

As we have already noted, nonstoichiometric and/or doped oxides are high temperature systems, since solid solutions are stable at relatively high temperatures only. At lower temperatures the high free energy related to the high concentration of defects (oxygen vacancies, guest ions) can be reduced either by defects ordering and their localization as structural elements (superstructures formation), or by their elimination or precipitation (nanostructuring, microdomain texturing) [1]. The difference between the MDT phases and ordered superstructures is that in MDT oxides part of disorder is already accumulated at low temperatures as excess interfacial energy (disordered lattice in the vicinity of interfaces). Therefore, the lower is working temperature, the more essential is the MDT oxide advantage with regard to oxygen transport. That is why MDT oxides are promising materials for low and moderate temperature oxidative catalysis, oxygen permeable membranes for partial oxidation of hydrocarbons, SOFC's electrodes, sensors etc.

With our developed model, we have shown that nanostructuring allows inhomogeneous oxygen diffusion in domains and along the interfaces; the difference in diffusion coefficients may attain several orders of magnitude. The most important issue is that stationary flux of oxygen ions through a MDT perovskite membranes at temperatures lower than the point of order-disorder transition is determined mostly by coefficient  $D_2$ .

Since activation energy  $E_a$ , necessary for the oxygen ions migration along the grain boundaries (g.b.), may be essentially lower than that for the bulk (b.) diffusion,  $E_a(\text{g.b.}) \sim 1/2 E_a(\text{b.})$  [23], oxygen permeable membranes made of MDT oxides are able to provide several orders of magnitude higher oxygen fluxes at the working temperatures below the order-disorder transition point. Let us mention though that nanostructuring is not the sufficient condition for intensive oxygen transport along the interfaces. For example, alkali/rare earth manganites possess a well-developed microstructure, but oxygen mobility in them is very low, whereas alkali/rare earth ferrites, and in particular cobaltites show unusually high oxygen transport [8]. Apparently, the transport properties of oxides are influenced by the interfacial energy, which is dependent on a set of parameters (M–O bond strength, coordination of cations, their charges and size, electronic configuration, magnetic state of cations, etc.). In case if interfacial energy is high enough (disordered interface), one may expect high permeability of oxygen. If interface is ordered (low interfacial energy), most likely it will be a barrier for the ion diffusion.

We shall further study the kinetics of MDT perovskites oxidation at various temperatures to determine the activation energy for oxygen ions migration along the interfaces and inside the domains and develop the method for mea-

asuring oxygen diffusion parameters in the nanostructured materials. Comparing the data obtained at low temperature by means of relatively simple wet electrochemical technique with the data related to oxygen permeability at high temperatures, we might define the mechanism of oxygen transport in MDT oxides, elucidate the factors determining the high values of oxygen fluxes in these materials and might open strategies to develop new oxygen-conducting materials operating at moderate temperature.

## References

- [1] J.S. Anderson, The thermodynamics and theory of nonstoichiometric compounds, in: A. Rabenau, (Ed.), *Problems of Nonstoichiometry*, North-Holland Publ. Co, Amsterdam, 1970, p.1.
- [2] H. Schmalzried, in: H.F. Ebel (Ed.), *Solid State Reactions*, Verlag Chemie, 1981, p.167.
- [3] S.C. Tjong, Haydn Chen, *Materials Science and Engineering* **R 45** (2004) 1–88.
- [4] E. Dagotto, T. Hotta, A. Moreo, *Physics Reports* **344** (2001) 1–153.
- [5] M.Á. Alario-Franco, J.M. Gonzalez-Calbet, M. Vallet-Regi, J.-C. Grenier, *J. Solid State Chem.* **49** (1983) 219.
- [6] J. Maier, *Prog. Solid State Chem.* **23** (1995) 171-263.
- [7] R. Würschum, *Rev. Metall.* **96** (1999) 1547.
- [8] H.J.M. Bouwmeester, A.J. Burggraaf, Dense ceramic membranes for oxygen separation, in: A.J. Burggraaf and L. Cot (Eds.), *Fundamentals of Inorganic Membrane Science and Technology*, Elsevier, Amsterdam, 1996, p. 435.
- [9] A. Nemudry, E.L. Goldberg, M. Aguirre and M.A. Alario-Franco, *Solid State Sciences* **4** (2002) 677.
- [10] P. Fenshom, *Australian Just. Sc. Research* **3** (1950) 105.
- [11] M. K. Achter and R. Smoluchowski, *Phys. Rev.* **76** (1949) 470.
- [12] R. E. Hofmann and D. Turnbull, Lattice and grain-boundary self-diffusion in silver, *Journ. of Appl. Phys.* **22** No. 5 (1951) 634.
- [13] J.C. Fisher, *J. Appl. Phys.* **22** (1951) 74.
- [14] B.S. Bokshstein, A.I. Magidson and I.L. Svetlov, *Fizika Metallov i Metallovedenie* **6** (1958) 1040. In Russian.
- [15] Ya. E. Gegusin. *Macroscopic defects in metals* (Moscow, 1962). In Russian.
- [16] R.T.P. Whipple, *Phil. Mag.* **45** (1954) 1225.

- [17] E. Goldberg, A. Nemudry, V. Boldyrev, R. Schöllhorn, *Solid State Ionics* **110** (1998) 223.
- [18] E. Goldberg, A. Nemudry, V. Boldyrev, R. Schöllhorn, *Solid State Ionics* **122** (1999) 17.
- [19] S. Sunde, K. Nişancioğlu, T. M. Gür, *J. Electrochem. Soc.* **143** No. 11 (1996) 3497.
- [20] C. J. Wen, C. Ho, B. A. Boukamp, I. D. Raistick, W. Weppner, and R. A. Huggins, *Int. Metals Rev.* No. 5 (1981) 253.
- [21] B. Hüpper and E. Pollak, A new method for numerical inversion of the Laplace transform, physics/9807051.
- [22] P. Glyanenko, A. Nemudry, Z.R. Ismagilov and H.J.M. Bouwmeester, Investigation of structure, phase transition and oxygen mobility in  $\text{SrCo}_{0.8-x}\text{Fe}_{0.2}\text{Ta}_x\text{O}_{3-y}$  mixed conductors, in preparation.
- [23] P. Kofstad, *High temperature corrosion*, Elsevier, London, 1988, 558p.